Article

Neuron

Clock Genes Control Cortical Critical Period Timing

Highlights

- Circadian gene oscillation emerges postnatally in mouse visual cortex
- Clock genes regulate parvalbumin-circuit maturation and critical period onset
- Clock defects in cortical plasticity are reversible by enhanced GABA signaling
- Parvalbumin cell-intrinsic clock genes are necessary for critical period timing

Authors

Yohei Kobayashi, Zhanlei Ye, Takao K. Hensch

Correspondence

hensch@mcb.harvard.edu

In Brief

The function of circadian Clock genes outside the SCN remains poorly understood. Kobayashi et al. show that Clock genes within parvalbumin-cells are important for their maturation and subsequent timing of critical period plasticity in the neocortex.

Accession Numbers

GSE62956

Kobayashi et al., 2015, Neuron *86*, 1–12
April 8, 2015
http://dx.doi.org/10.1016/j.neuron.2015.02.036

CellPress

Please cite this article in press as: Kobayashi et al., Clock Genes Control Cortical Critical Period Timing, Neuron (2015), http://dx.doi.org/10.1016/j.neuron.2015.02.036

Neuron
Article

CellPress

Clock Genes Control Cortical Critical Period Timing

Yohei Kobayashi,[1,2] Zhanlei Ye,[1] and Takao K. Hensch[1,2,*]
[1]Center for Brain Science, Department of Molecular Cellular Biology, Harvard University, 52 Oxford Street, Cambridge, MA 02138, USA
[2]F.M. Kirby Neurobiology Center, Department of Neurology, Boston Children's Hospital, Harvard Medical School, 300 Longwood Avenue, Boston, MA 02115, USA
*Correspondence: hensch@mcb.harvard.edu
http://dx.doi.org/10.1016/j.neuron.2015.02.036

SUMMARY

Circadian rhythms control a variety of physiological processes, but whether they may also time brain development remains largely unknown. Here, we show that circadian clock genes control the onset of critical period plasticity in the neocortex. Within visual cortex of *Clock*-deficient mice, the emergence of circadian gene expression was dampened, and the maturation of inhibitory parvalbumin (PV) cell networks slowed. Loss of visual acuity in response to brief monocular deprivation was concomitantly delayed and rescued by direct enhancement of GABAergic transmission. Conditional deletion of *Clock* or *Bmal1* only within PV cells recapitulated the results of total *Clock*-deficient mice. Unique downstream gene sets controlling synaptic events and cellular homeostasis for proper maturation and maintenance were found to be mis-regulated by *Clock* deletion specifically within PV cells. These data demonstrate a developmental role for circadian clock genes outside the suprachiasmatic nucleus, which may contribute mis-timed brain plasticity in associated mental disorders.

INTRODUCTION

Neural circuits are shaped by experience-dependent plasticity in early postnatal life (Hensch, 2004). A classic example is the enduring loss of visual acuity, known as amblyopia, upon sensory deprivation of one eye during a limited developmental window (Wiesel, 1982). The maturation of cortical inhibitory networks in the postnatal brain is important for initiating this critical period (Fagiolini and Hensch, 2000; Sugiyama et al., 2008). One particular GABA cell-type, fast-spiking neuron expressing parvalbumin (PV) is pivotal for this process (Fagiolini et al., 2004; Hensch, 2005). In mouse primary visual cortex (V1), functional PV cell networks emerge after eye opening (>postnatal day [P] 12) and mature over 3 weeks (>P35) (Gonchar et al., 2007). With PV cell maturation, perineuronal nets (PNNs) of extracellular matrix molecules condense around their somata, which in turn contributes to closure of critical period plasticity (Beurdeley et al., 2012; Carulli et al., 2010; Pizzorusso et al., 2002).

Direct manipulation of the local extracellular milieu surrounding cortical PV cells can influence plasticity timing. Acceleration of PV cell maturation by overexpressing non-cell-autonomous factors, such as brain-derived neurotrophic factor (BDNF) or orthodenticle homeobox 2 (Otx2), induces precocious plasticity (Huang et al., 1999; Sugiyama et al., 2008). In contrast, removing PNNs or reducing Otx2 uptake reopens plasticity in adulthood (Beurdeley et al., 2012; Pizzorusso et al., 2002; Spatazza et al., 2013).

Circadian rhythms are approximately 24 hr biological clocks that drive daily patterns of gene expression, physiology, and behavior in most organisms (Dibner et al., 2010; Masri and Sassone-Corsi, 2010; Takahashi et al., 2008). In mammals, the central oscillator is located in the hypothalamic suprachiasmatic nucleus (SCN) and is generated by an auto-regulatory genetic feedback loop driven by the transcription factors CLOCK and BMAL1 (Lowrey and Takahashi, 2011) (Figure 1A). This transcriptional loop can be observed not only in the SCN but also in nearly all mammalian tissues (Dibner et al., 2010; Takahashi et al., 2008). Notably, the majority of brain regions exhibit circadian rhythmicity by the same oscillatory machinery (Wakamatsu et al., 2001; Yan et al., 2000). However, the purpose of circadian clocks outside the SCN, especially their link to higher-order functions such as information processing in the cerebral cortex, remains poorly understood.

In this study, we investigated a role for circadian clock genes in the binocular zone of mouse V1. We show that clock genes intrinsic to PV cells coordinate postnatal maturation of their networks and consequently the onset of critical period plasticity.

RESULTS

Circadian Gene Oscillation Emerges Postnatally in Mouse V1

We first examined in detail the development of cortical circadian rhythms by analyzing expression patterns in mouse V1 across various ages (Figure 1B). Quantitative RT-PCR (qRT-PCR) at multiple time points throughout the day/night cycle revealed that *Clock* expression did not show rhythmicity at any age (Figure 1C), consistent with previous reports in the SCN (Shearman et al., 2000) and forebrain (Dudley et al., 2003). However, rhythmicity of well-known circadian genes (*Dbp*, *Per1*, *Per2*) gradually emerged with age after eye opening and was fully established by adulthood (P70–P90) (Figure 1D). This developmental trajectory of molecular rhythm

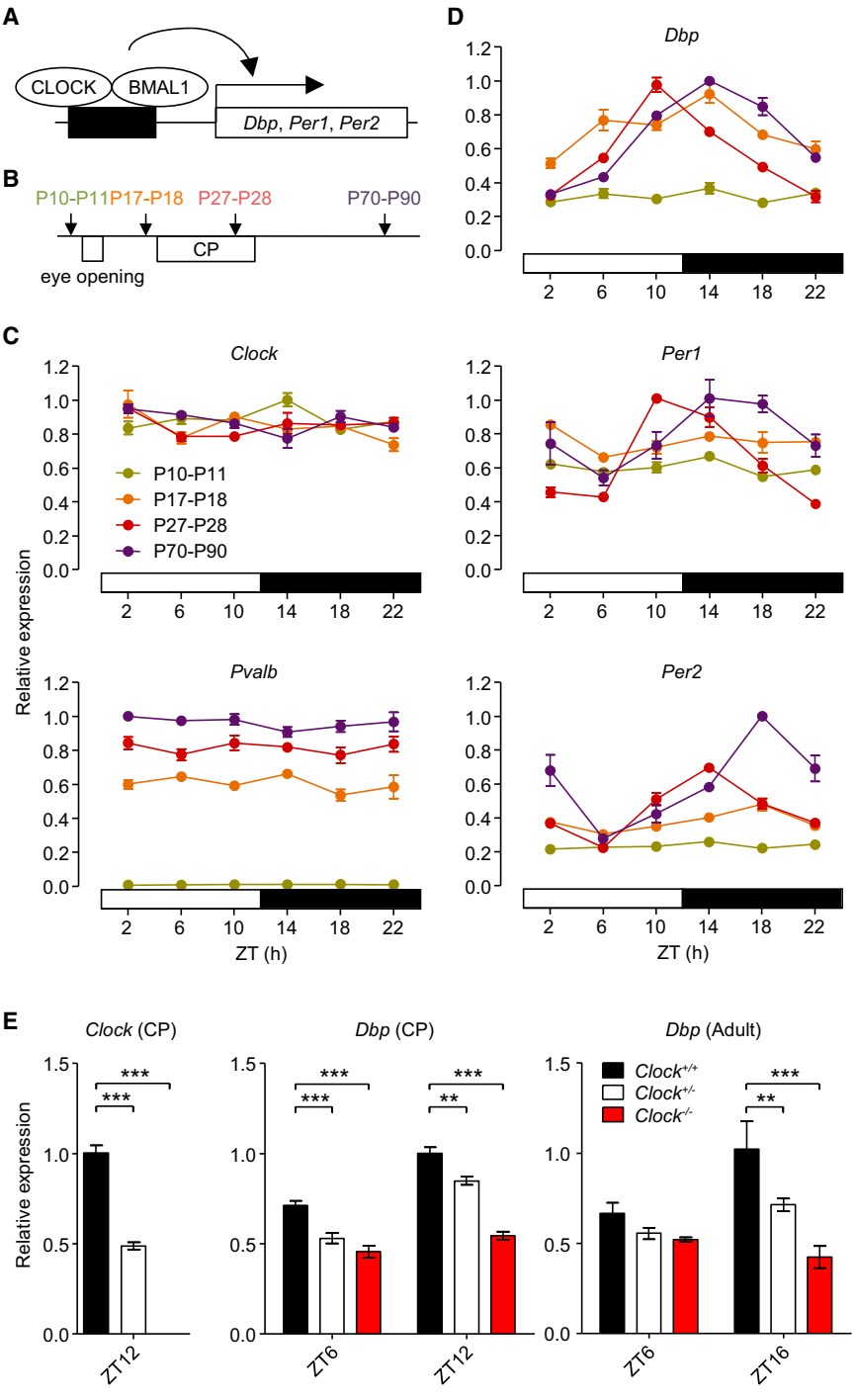

Figure 1. Postnatal Emergence of Molecular Circadian Oscillations in Mouse V1

(A) Schematic of CLOCK:BMAL1-mediated circadian gene expression.

(B) Assessment of circadian mRNA expression profile (three mice per time point) in primary visual cortex (V1) just before eye opening (P10–P11), at pre-critical period (CP) (P17–P18), CP (P27–P28), and adult ages (P70–P90).

(C) Neither *Clock* nor *Pvalb* mRNA expression exhibit circadian rhythmicity at any age. ZT, zeitgeber time.

(D) Circadian expression patterns for *Dbp*, *Per1*, and *Per2* mRNAs emerge after eye opening.

(E) Genetic reduction of *Clock* (exon 5–6) or *Dbp* mRNA expression in V1 at CP (P27–P30, 4–6 mice) or adult ages (P70–P90, 3–5 mice). $^{**}p < 0.01$; $^{***}p < 0.001$ (one-way ANOVA, Dunnett's post hoc analysis for *Clock*; two-way ANOVA, Bonferroni's post hoc analysis for *Dbp*). Values are mean ± SEM.

was relatively late compared to that in the SCN which appears perinatally (Shimomura et al., 2001).

Due to the concurrent development of circadian oscillations with onset of the visual critical period, we hypothesized a direct impact upon cortical plasticity during early postnatal life. To examine such a developmental role, we took advantage of mutant mice whose circadian gene expression is dampened. Among the two core clock components, CLOCK and BMAL1, we chose *Clock*-deficient ($Clock^{-/-}$) mice (Debruyne et al., 2006), because total *Bmal1*-deficient animals exhibit a variety of defects including reduced total activity and age-dependent weight loss (Bunger et al., 2000; Kondratov et al., 2006), which could affect brain functions independently. No gross abnormalities were observed in $Clock^{-/-}$ mice, as reported previously (Debruyne et al., 2006). We first verified attenuation of circadian gene expression within V1 of $Clock^{-/-}$ mice. Near the circadian peak (zeitgeber time [ZT] 12 at critical period; ZT16 in adulthood) or trough (ZT6), qRT-PCR analyses revealed *Dbp* expression to be reduced in a dose-dependent manner of *Clock* deletion (Figure 1E), confirming a dampened circadian gene expression in V1 of $Clock^{-/-}$ mice.

CLOCK Determines Critical Period Timing

To assess the impact of *Clock* deletion on critical period plasticity, we measured visual acuity following 4 days of monocular deprivation (MD) using visual-evoked potential (VEP) recordings, as reported previously in mice (Beurdeley et al., 2012; Carulli et al., 2010; Kang et al., 2013; Morishita and Hensch, 2008). VEP amplitudes were measured in response to various stimulus spatial frequencies and visual acuity calculated by linear extrapolation (log coordinates) to zero amplitude (Figures 2A, 2B, 2D, and 2E). The latency to VEP onset, which is largely determined by retino-geniculate processing, and baseline visual acuity of $Clock^{-/-}$ mice were comparable to those of age-matched $Clock^{+/+}$ controls (Figures 2C, 2F, and S1A).

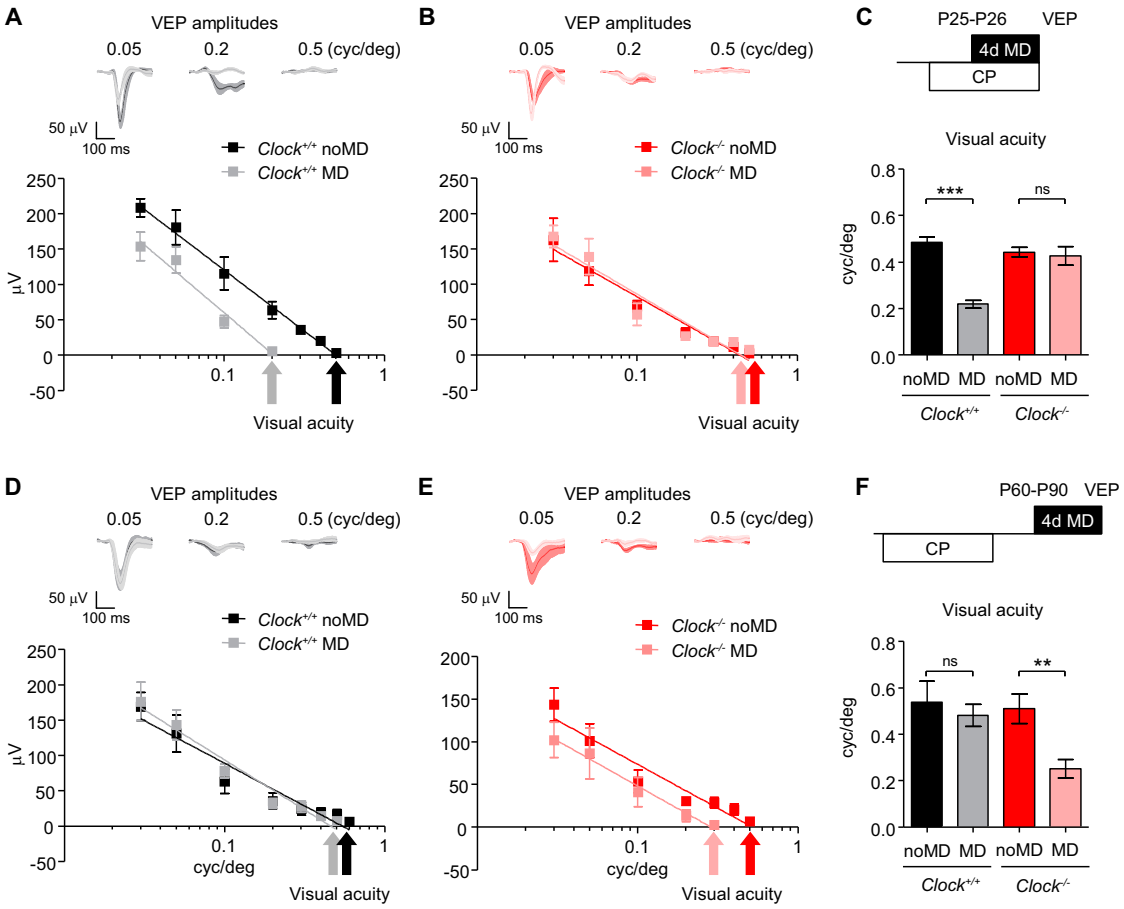

Figure 2. Delayed Critical Period Plasticity in *Clock*$^{-/-}$ Mice

(A–C) Monocular deprivation (MD) performed for 4 days during the typical CP from P25–P26. Averaged VEP traces and amplitudes in *Clock*$^{+/+}$ (noMD and MD, 5 mice each) (A) and *Clock*$^{-/-}$ mice (noMD, 5 mice; MD, 6 mice) (B). Visual acuity per mouse was determined by extrapolating VEP amplitude data to 0 V and averaged (C). ***$p < 0.001$; ns, not significant (t test). Values are mean ± SEM.

(D–F) MD performed for 4 days in adulthood (P60–P90). Averaged VEP traces and amplitudes in *Clock*$^{+/+}$ (noMD and MD, 5 mice each) (D) and *Clock*$^{-/-}$ mice (noMD and MD, 5 mice each) (E) and evaluated visual acuity (F). **$p < 0.01$; ns, not significant (t test). Values are mean ± SEM. See also Figures S1, S2, and S3.

In addition, eye-specific segregation of retino-geniculate axon terminals in the dorsal lateral geniculate nucleus (dLGN), which is refined earlier postnatally in an activity-dependent manner (Huberman et al., 2008), was also normal in *Clock*$^{-/-}$ mice (Figures S1C and S1D). Taken together, the subcortical visual pathway in *Clock*$^{-/-}$ mice appeared intact.

Upon MD during the critical period starting from P25–P26, visual acuity of the deprived eye was significantly reduced (i.e., amblyopia) in *Clock*$^{+/+}$ mice, indicating strong plasticity at this age (Figures 2A and 2C). However, visual acuity was not changed in *Clock*$^{-/-}$ mice (Figures 2B and 2C). Instead, after MD in adulthood starting from P60–P90, visual acuity remained typically unchanged in *Clock*$^{+/+}$ mice but was significantly reduced in *Clock*$^{-/-}$ mice (Figures 2D–2F). This delayed onset of visual plasticity was also confirmed by a delayed ocular dominance shift (contra/ipsi ratio at low spatial frequency) following MD in *Clock*$^{-/-}$ mice (Figures S2A and S2B). Moreover, the peak plastic window in *Clock*$^{-/-}$ mice was also effectively prolonged in duration (>2 months) as compared to that of a normal critical period (<1 month), because amblyopia was still inducible at >P120 in the mutants (Figure S3A).

Since maturation of cortical inhibitory networks in the postnatal brain is important for initiating this critical period (Fagiolini and Hensch, 2000; Sugiyama et al., 2008), we hypothesized that inhibition might be compromised in *Clock*$^{-/-}$ mice. Thus, we attempted to rescue critical period timing by enhancing GABAergic transmission using benzodiazepine agonists (Fagiolini and Hensch, 2000). Amblyopia was induced fully by diazepam treatment concurrent with MD at P25–P26 in *Clock*$^{-/-}$ mice (Figures 3A and 3B). Moreover, mimicking a critical period by 10-day injection (P23–P33) of diazepam (Fagiolini and Hensch, 2000) prevented later adult plasticity in *Clock*$^{-/-}$ mice (Figure 3C). These data suggested a reduced inhibition within local cortical circuits in the total absence of CLOCK (Hensch et al., 1998).

CLOCK Regulates Maturation of PV Cell Circuits

We examined a panel of neural markers for excitatory (*Camk2a*) or inhibitory (*Pvalb*, parvalbumin; *Sst*, somatostatin; *Calb1*,

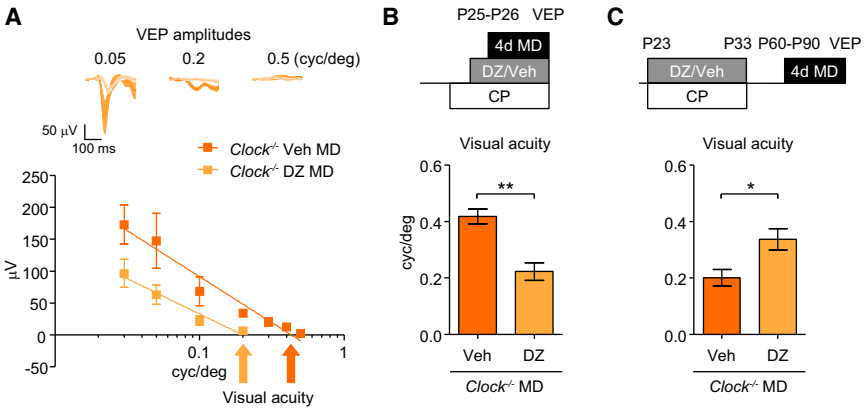

Figure 3. Restored Critical Period Plasticity by Enhanced GABA Signaling in *Clock*$^{-/-}$ Mice

(A and B) *Clock*$^{-/-}$ mice treated with diazepam (DZ, 5 mice) or vehicle solution (Veh, 4 mice) starting 1 day before and concurrent with MD for 4 days from P25–P26. Averaged VEP traces and amplitudes (A) and evaluated visual acuity (B). **p < 0.01 (t test). Values are mean ± SEM

(C) Visual acuity in *Clock*$^{-/-}$ mice treated with DZ (6 mice) or Veh (4 mice) from P23 to P33 prior to 4 days MD at P60–P90. *p < 0.05. Values are mean ± SEM.

calbindin; *Calb2*, calretinin) neurons. Only the expression of *Pvalb* was significantly reduced at both critical period and adult ages in *Clock*$^{-/-}$ mice (Figure 4A). Because *Pvalb* expression itself did not show circadian rhythmicity during development (Figure 1C), it is unlikely that the *Pvalb* gene is a direct target of CLOCK:BMAL1-mediated transcription. Moreover, intrinsic electrophysiological properties of PV cells were unaffected by *Clock* deletion (Figure S4 and Table S1). Instead, immunohistological analysis revealed the number of PV cells to be reduced in *Clock*$^{-/-}$ mice (Figures 4B and 4C) and also in heterozygous *Clock*$^{+/-}$ mice (107.08 ± 5.1 cells/mm^2 at critical period, p < 0.01 compared to *Clock*$^{+/+}$ mice, 4 mice each, t test). PV cell circuits remained immature even at >P120 in *Clock*$^{-/-}$ mice (Figures S3B and S3C), which was consistent with their prolonged plasticity (Figure S3A).

The maturation of soma-enwrapping PNNs was also slowed in *Clock*$^{-/-}$ mice (Figures 4B, 4D, and 4E) and may contribute to their plasticity in adulthood (Figures 2E and 2F; Pizzorusso et al., 2002). Detailed analysis further revealed PV-positive puncta onto layer 4 pyramidal neurons to be decreased in size and number in *Clock*$^{-/-}$ mice (Figures 5A–5C). Moreover, we analyzed another marker for PV puncta, Synaptotagmin-2 (Syt2) (Figure S5A), which is neither activity (Sommeijer and Levelt, 2012) nor circadian dependent (Figure S5B). Syt2 puncta were also decreased in size and number in *Clock*$^{-/-}$ mice (Figures 5D–5F). Consistent with these anatomical changes, the frequency (but not amplitude) of miniature inhibitory post-synaptic currents (mIPSCs) was significantly reduced within layer 4 pyramidal neurons (Figures 5G–5I). Taken together, CLOCK is important for the functional maturation of PV cell circuits.

CLOCK Deletion Alters Expression of Unique Gene Sets within PV Cells

As circadian rhythmicity in cortical inhibitory interneurons has not been well-documented, we immunohistologically examined expression of molecular clock components in the inhibitory neurons of the binocular zone (V1b). CLOCK was expressed in more than 80% of PV cells but in only a smaller proportion of other interneuron subtypes (38% and 45% in somatostatin (SST)- and calretinin (CR)-positive interneurons, respectively), suggesting a predominant function for CLOCK in PV cells (Figures S6A and S6B). A circadian gene product PER1 globally exhibited circadian rhythmicity with a peak at ZT0 and a trough at ZT12 (Figure S6C), and the expression level of PER1 was dampened in *Clock*$^{-/-}$ mice (Figure S6D). This PER1 profile was similar within PV cells (Figure S6E), indicating a functional CLOCK-mediated circadian machinery within PV cells.

We next asked which downstream genes might be responsible for the poor maturation of PV cell circuits, using microarray analysis of fluorescence-activated cell-sorted PV cells (Figure 6A). Gene ontology (GO) analysis of transcripts expressed differentially upon *Clock* deletion (Figure 6B) revealed an over-representation of GO terms related to synaptic function (Cluster 1), mitochondrial function (Cluster 2), and ATPase activity (Cluster 3) (Figure 6C). These results suggest that CLOCK may regulate unique sets of genes controlling synaptic events and cellular homeostasis for the proper maturation and maintenance of PV cells.

PV Cell-Intrinsic Clock Genes Set Critical Period Timing

To determine whether the role of circadian clock genes on PV cell maturation is cell autonomous, we performed conditional deletion of *Clock* from PV cells using *Clock*^{flox} mice (Debruyne et al., 2006) crossed to a *PV-Cre* line expressing Cre recombinase driven by the parvalbumin promoter (Madisen et al., 2010). Immunohistological analysis confirmed specific loss of CLOCK expression within cortical PV cells at typical critical period age (Figure 7A). Importantly in the SCN, PV was not expressed, leaving CLOCK expression intact by our conditional deletion (Figure 7B). Analyses by immunohistochemistry and qRT-PCR again revealed PV cell circuits and surrounding PNNs to be significantly immature at critical period and adult ages by the conditional deletion of *Clock* (Figures 7C–7H). While amblyopia was then induced as expected by brief MD in *PV-Cre* control littermates only at critical period, visual acuity was significantly reduced in *PV-Cre; Clock*$^{f/f}$ mice by brief MD only in adulthood (Figure 7I).

To verify these results, we deleted another core clock component, BMAL1 (Figure 1A), just from PV cells using *Bmal1*^{flox} mice (Storch et al., 2007), which caused neither gross abnormalities associated with global deletion (Bunger et al., 2000; Kondratov et al., 2006) nor deficits in retino-cortical transmission (Figure S1B). Reduction of *Pvalb* expression was more prominent in the conditional knockout of *Bmal1* than that of *Clock*

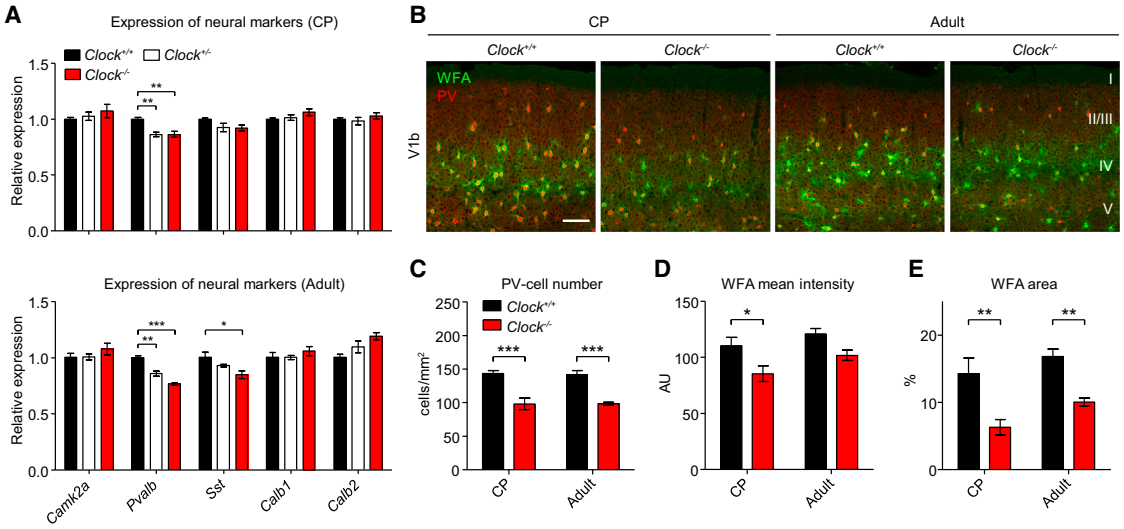

Figure 4. Delayed PV Cell Maturation in *Clock*$^{-/-}$ Mice

(A) mRNA expression of *Camk2a*, *Pvalb*, *Sst*, *Calb1*, and *Calb2* in V1 at CP (P27–P30, 4–6 mice) or adult ages (P70–P90, 3–5 mice). *p < 0.05; **p < 0.01; ***p < 0.001 (one-way ANOVA, Dunnett's post hoc analysis). Values are mean ± SEM.

(B–E) PV cells and WFA-stained perineuronal nets in the binocular zone of primary visual cortex (V1b) at CP (P29) and adult ages (P60–P80) (B). Decreased number of PV cells (C), WFA mean intensity (D), and WFA area (E) in *Clock*$^{-/-}$ mice quantified at CP (*Clock*$^{+/+}$, 4 mice; *Clock*$^{-/-}$, 3 mice) or adult ages (*Clock*$^{+/+}$, 3 mice; *Clock*$^{-/-}$, 6 mice). Scale bar, 100 μm. AU, arbitrary units. *p < 0.05; **p < 0.01; ***p < 0.001 (two-way ANOVA, Bonferroni's post hoc analysis). Values are mean ± SEM. See also Figure S3.

(Figure 7H), perhaps because *Bmal1* deletion has a stronger impact on circadian rhythmicity (Bunger et al., 2000; Debruyne et al., 2006). Visual acuity again remained unchanged by MD at typical critical period ages (Figure S7D) but was reduced significantly in adulthood in *PV-Cre; Bmal1*$^{f/f}$ mice (Figure 7I). These results recapitulate delayed onset of plasticity identified in global *Clock*$^{-/-}$ mutants by selective deletion of *Clock* or *Bmal1* only from PV cells.

For comparison, we also generated excitatory neuron-specific *Bmal1* deletion using *TLCN-Cre* mice in which Cre recombinase is expressed only in forebrain pyramidal neurons (Mitsui et al., 2007). We confirmed restricted loss of BMAL1 expression from excitatory neurons in cortical layers 2/3 and 5/6 and not in the SCN (Figures S7A and S7B). As opposed to PV cell-specific deletion, the removal of *Bmal1* from the more numerous excitatory neuron population neither reduced *Pvalb* expression nor delayed critical period plasticity (Figures S7C and S7D). Taken together, intrinsic clock genes within pivotal PV cells are important for their maturation and subsequent timing of critical period plasticity (Figure S8).

DISCUSSION

Circadian rhythms have been shown to control not only daily biological processes but also the timing of other physiological events outside the diurnal cycle. For example, there is a link between circadian timing mechanisms and seasonal, photoperiodic-driven changes in an organism's physiology and behavior (Golombek et al., 2014). However, there is little evidence to date demonstrating a role of the circadian system in timing of developmental processes.

In this study, we showed that circadian clock genes time postnatal brain development. Moreover, the necessary clockwork is cell intrinsic to specific interneurons known to play a pivotal role in critical period plasticity (Hensch, 2005). Circadian gene oscillation in mouse V1 emerged in register with PV cell maturation, which was anatomically and functionally slowed by disruption of the molecular clock. Concomitantly, the onset of critical period plasticity was delayed but restored by pharmacological enhancement of GABAergic transmission.

The developmental delay observed here is not likely due to loss of systemic circadian rhythms, since *Clock*$^{-/-}$ mice exhibit normal behavioral rhythms under a conventional light:dark cycle (Debruyne et al., 2006), and PV cell-specific *Clock* or *Bmal1* conditional knockout mice also exhibited delayed critical period timing despite an intact master clock in the SCN (Figure 7). However, it is important to keep in mind that the levels and/or activity of CLOCK:BMAL1 are tightly linked to circadian oscillations, which are disrupted by pulsed-light exposure or sleep deprivation suppressing CLOCK:BMAL1-mediated transcription (Grone et al., 2011; Mongrain et al., 2011). Thus, these environmental influences even during normal development may still impact timing of critical period plasticity through the mechanisms described here.

What is the molecular machinery underlying PV circuit maturation? Because CLOCK:BMAL1-mediated transcription targets a variety of genes in different cellular contexts across tissues (Janich et al., 2011; Marcheva et al., 2010; Paschos et al., 2012; Yu et al., 2013), PV cell-specific target genes or other mechanisms controlled by the clock machinery should be considered. Our PV cell-specific microarray analysis identified unique sets of genes mis-regulated in *Clock*$^{-/-}$ mice that are

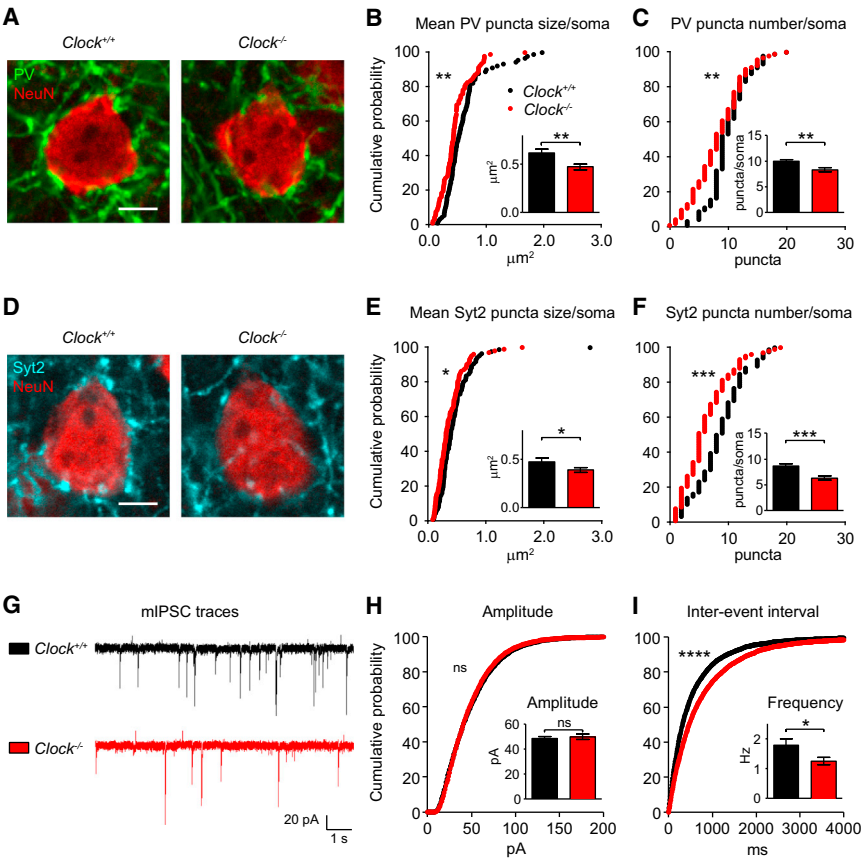

Figure 5. Functionally Weakened PV Circuits in *Clock*$^{-/-}$ Mice

(A–C) Immature PV puncta onto pyramidal neurons in layer 4 of V1b in *Clock*$^{-/-}$ mice at CP (P29) (A). Cumulative plots for mean PV puncta size per soma (B) and PV puncta number per soma (C), and their mean values (insets) in *Clock*$^{+/+}$ (90 cells from 4 mice) and *Clock*$^{-/-}$ mice (92 cells from 4 mice). (D–F) Immature Syt2 puncta onto pyramidal neurons in layer 4 of V1b in *Clock*$^{-/-}$ mice at CP (P29) (D). Same analyses as in (B) and (C) in *Clock*$^{+/+}$ (86 cells from 4 mice) and *Clock*$^{-/-}$ mice (102 cells from 4 mice). Scale bar, 5 μm. *p < 0.05; **p < 0.01; ***p < 0.001 (K-S test for cumulative plots; Mann-Whitney test for insets). Values are mean ± SEM. (G–I) mIPSC traces from pyramidal neurons in layer 4 of V1b in *Clock*$^{+/+}$ (21 cells from 3 mice) and *Clock*$^{-/-}$ mice (23 cells from 3 mice) at CP (P26–P28) (G). Cumulative plots for mIPSC amplitude (H) and inter-event interval (I) from all events, and their mean values from all cells (insets). ****p < 0.0001 (K-S test); *p < 0.05 (Mann-Whitney test for insets); ns, not significant. Values are mean ± SEM. See also Figures S4 and S5 and Table S1.

potentially responsible for the immature PV cell circuits. It is likely that these genes are involved in maturation and/or maintenance of PV cell circuits rather than earlier events such as cell migration. Notably, circadian gene oscillations first emerged in V1 after eye opening, and the delayed deletion of *Clock* or *Bmal1* once PV cells have already appeared induced similar phenotypes as seen by constitutive *Clock* deletion. Here, we discuss three potential mechanisms that might then influence PV circuit maturation.

First, clock machinery could directly control synaptic input and/or output of PV cells. Enhancing neuromodulatory action, such as acetylcholine or serotonin, has been shown to reopen adult plasticity (Maya Vetencourt et al., 2008; Morishita et al., 2010). Reduced expression of *Lynx1* or *Htr2a* observed in *Clock*-deleted PV cells (Figure 6) may then alter excitatory-inhibitory (E/I) balance in the surrounding circuitry. Lynx1-mediated dampening of cholinergic signaling would normally limit adult plasticity (Morishita et al., 2010). Altered 5-HT$_{2A}$-mediated serotonin signaling within PV cells may likewise modulate E/I balance by adjusting spontaneous IPSC frequency onto pyramidal neurons (Weber and Andrade, 2010).

As for PV cell output, presynaptic neurexins (NRXNs) bind to neuroligins (NLGNs) expressed on the target postsynapic site and mediate signaling across the synapse (Südhof, 2008). Disruption of specific NRXN-NLGN complexes weakens inhibitory synapses formed by PV cells (Chubykin et al., 2007). Interestingly, *Nrxn* transcripts display circadian oscillations in the SCN (Shapiro-Reznik et al., 2012), suggesting a direct involvement of CLOCK:BMAL1-mediated transcription. Altered expression of NRXNs (*Nrxn1*, *Nrxn2*, *Nrxn3*) in *Clock*-deleted PV cells (Figure 6) may underlie the reduced inhibitory output onto pyramidal neurons observed in *Clock*$^{-/-}$ mice (Figure 5).

Second, circadian clock genes may preserve PV cell integrity. Circadian rhythms have been shown to regulate redox homeostasis in the brain, and disruption of circadian genes causes neuronal oxidative damage (Musiek et al., 2013). Notably, fast-spiking PV cells are highly metabolically active with a hallmark of abundant mitochondrial molecules (Plessy et al., 2008) and are particularly vulnerable to redox dysregulation as compared to other neuronal types, resulting in their enhanced oxidative stress and loss of PNNs (Cabungcal et al., 2013a, 2013b). Direct cell-autonomous redox dysregulation by deletion of the primary antioxidant (glutathione) synthetic enzyme (*Gclc*) only within PV cells is sufficient to prolong critical period plasticity (Morishita et al., 2015). Altered expression of genes downstream of CLOCK related to the respiratory chain (e.g., *Cox* and *Nduf* family genes) and redox regulation (e.g., *Gpx4*) (Figure 6, Cluster 2) may thus jeopardize the integrity of redox homeostasis. Another important PV circuit maturation and maintenance factor in this context is Otx2 (Beurdeley et al., 2012; Spatazza et al., 2013; Sugiyama et al., 2008). How this non-cell-autonomous molecule interacts with PV cell-intrinsic clocks will be of great interest, as Otx2 has been suggested to reciprocally interact with CLOCK in a positive regulatory loop in *Xenopus* embryos (Green et al., 2001; Morgan, 2002).

Third, apart from the molecular targets above, the clock system itself may act as a PV cell-intrinsic timer. Intracellular

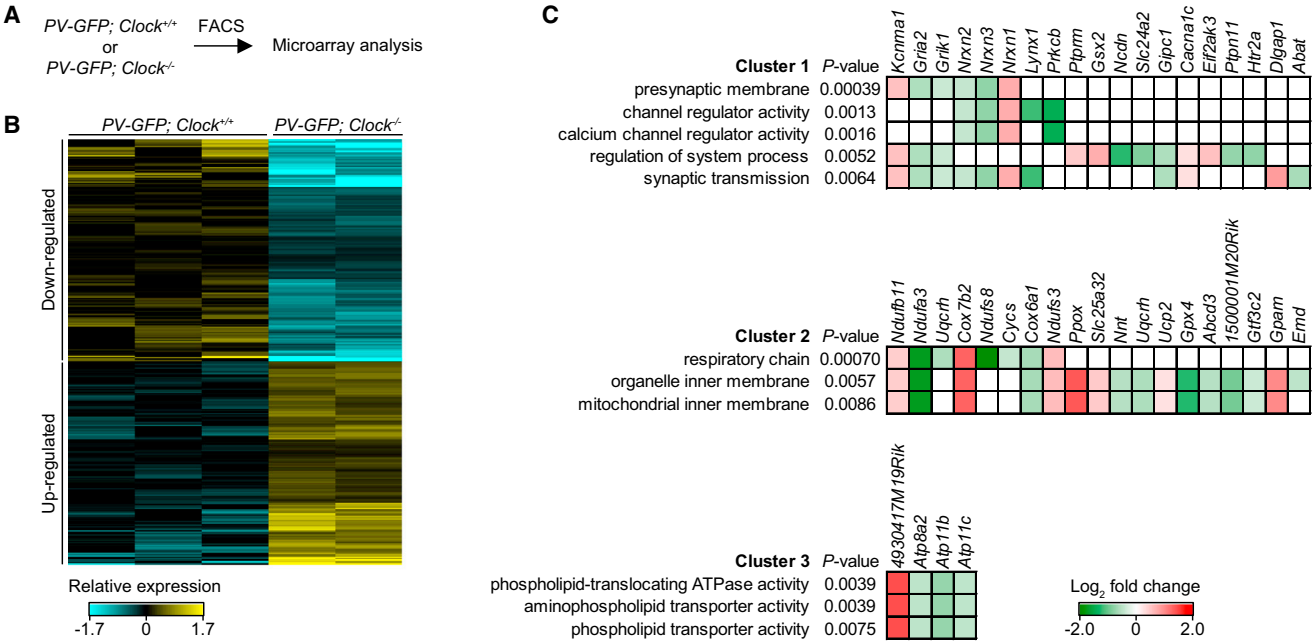

Figure 6. Candidate Genes Influencing PV Circuit Maturation in *Clock*$^{-/-}$ Mice

(A) Workflow of microarray analysis on adult (P60–P64) *PV-GFP; Clock*$^{+/+}$ (3 mice) and *PV-GFP; Clock*$^{-/-}$ mice (2 mice).

(B) Heatmap of probes differentially expressed by *Clock* deletion ($p < 0.05$, $\log_2$-fold change > 0.25 or < -0.25).

(C) Gene ontology (GO) analysis of genes differentially expressed by *Clock* deletion. GO terms were annotated and clustered using DAVID. Heatmap shows $\log_2$-fold change of genes annotated with given GO terms.

maturational programs in addition to the local cortical milieu may regulate the development of GABAergic circuits (Bartolini et al., 2013). Supporting this idea, when embryonic precursors of GABA neurons are transplanted into the postnatal visual cortex of mice, an ectopic critical period is induced once sufficient maturational time has elapsed for the transplanted cells (Southwell et al., 2010). Curiously, embryonic stem cells, which do not exhibit circadian rhythmicity, acquire their oscillatory machinery during neural differentiation (Yagita et al., 2010). Emergence of full circadian oscillations (i.e., over a certain number of cycles) may positively drive postnatal PV cell development. The three roles above are not mutually exclusive and may independently or coordinately aid proper maturation of PV cell circuits.

Lastly, our findings offer a neurodevelopmental link between circadian disruption and mental illness. Linkage studies in human patients have implicated circadian gene mutations and behavioral changes (e.g., sleep disturbances) in psychiatric disorders, such as autism and schizophrenia (Chemerinski et al., 2002; Wulff et al., 2010), which are in turn marked by impaired PV cell circuits (Gogolla et al., 2009; Le Magueresse and Monyer, 2013; Marín, 2012). It has been shown that a set of genes misregulated in our *Clock*-deleted PV cells are associated with autism (*Kcnma1*, *Nrxn1-3*, *Prkcb*, *Slc24a2*, *Cacna1c*, *Ptpn11*, *Htr2a*, *Abat*) and schizophrenia (*Cacna1c*, *Htr2a*) (Allen et al., 2008; Basu et al., 2009). Understanding the cell-specific role of molecular clocks within developing PV cells may offer novel therapeutic approaches and insights into the etiology of mental illness as a reflection of critical period dysregulation.

EXPERIMENTAL PROCEDURES

Mice

C57BL/6J (JAX 000664), *Clock*$^{\Delta 5\text{-}6}$ (JAX 010925) (Debruyne et al., 2006), *Pvalb-2A-Cre* (*PV-Cre*) (JAX 012358) (Madisen et al., 2010), *Clock*^{flox} (JAX 010490) (Debruyne et al., 2006), and *Bmal1*^{flox} (JAX 007668) (Storch et al., 2007) mice were purchased from Jackson Laboratory. Original *PV-GFP* mouse breeders were kindly provided by H. Monyer (Heidelberg University) (Meyer et al., 2002). *TLCN-Cre* mouse (*TLCN3.9-Cre* Line D) was kindly provided by Y. Yoshihara (RIKEN Brain Science Institute) (Mitsui et al., 2007). All mice were on a C57BL/6J background. Mice were maintained on a 12 hr:12 hr light:dark cycle and allowed free access to regular chow and water. Mice were randomly assigned to the experimental groups.

To obtain *Clock*$^{-/-}$ mice, heterozygous *Clock*$^{\Delta 5\text{-}6}$ (*Clock*$^{+/-}$) mice were crossed with each other. To obtain *Clock*$^{+/+}$ or *Clock*$^{-/-}$ mice expressing GFP in PV cells, we crossed *PV-GFP; Clock*$^{+/-}$ mice with *Clock*$^{+/-}$ mice to generate *PV-GFP; Clock*$^{+/+}$ or *PV-GFP; Clock*$^{-/-}$ mice. To obtain PV cell-specific *Clock* conditional knockouts, we avoided using *PV-Cre*-positive male mice because germline recombination frequently occurred in the *PV-Cre* testes (Kobayashi and Hensch, 2013). In detail, male *Clock*$^{f/+}$ mice were crossed with female *PV-Cre*$^{+/-}$*; Clock*$^{f/+}$ or *PV-Cre*$^{+/+}$*; Clock*$^{f/+}$ mice to generate *PV-Cre*$^{+/-}$*; Clock*$^{+/+}$ (*PV-Cre*), *PV-Cre*$^{+/-}$*; Clock*$^{f/+}$, or *PV-Cre*$^{+/-}$*; Clock*$^{f/f}$ mice. The same strategy was applied to generate PV cell-specific *Bmal1* conditional knockout mice.

To obtain excitatory neuron-specific *Bmal1* conditional knockouts, we avoided using *TLCN-Cre*-positive female mice because of frequent ectopic recombination in its progeny. In detail, male *TLCN-Cre; Bmal1*$^{f/+}$ or *TLCN-Cre; Bmal1*$^{f/f}$ mice were crossed with female *Bmal1*$^{f/+}$ or *Bmal1*$^{f/f}$ mice to generate *Bmal1*$^{f/f}$ or *TLCN-Cre; Bmal1*$^{f/f}$ mice. Mice exhibiting ectopic recombination were excluded from experiments. Animal housing and experimental procedures were approved (AEP28-19) following guidelines of the Harvard University Institutional Animal Care and Use Committee.

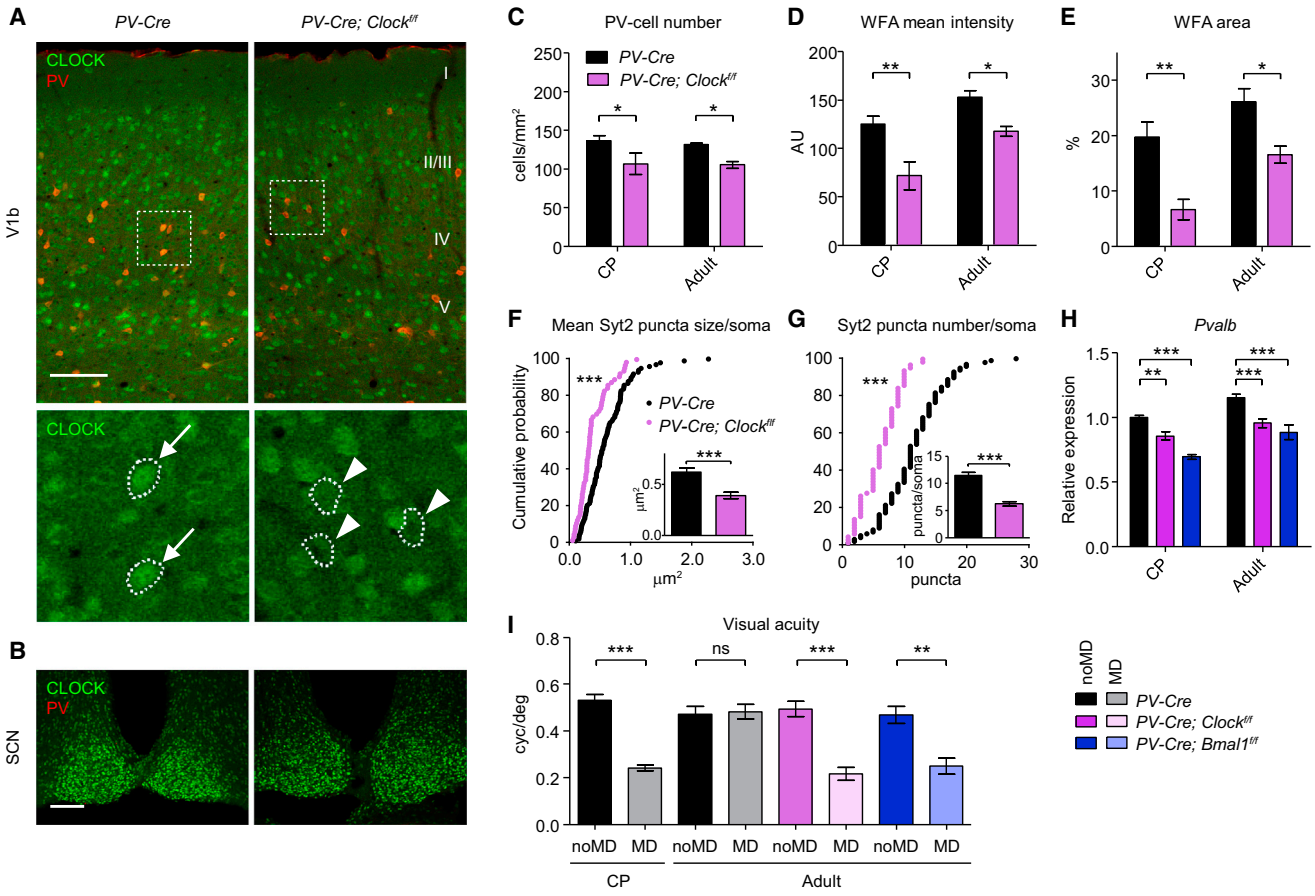

Figure 7. Delayed Plasticity by PV Cell-Specific *Clock* or *Bmal1* Deletion

(A) Conditional *Clock* deletion in V1b at P27 of *PV-Cre; Clock*$^{f/f}$ mice. Arrows, CLOCK-expressing PV cells. Arrowheads, CLOCK-depleted PV cells. Scale bar, 100 μm.

(B) CLOCK expression in the SCN at P66. Scale bar, 100 μm.

(C–E) PV cells and WFA-stained perineuronal nets in V1b at CP (P27) and adult ages (P60–P80). Decreased number of PV cells (C), WFA mean intensity (D), and WFA area (E) in *PV-Cre; Clock*$^{f/f}$ mice quantified at CP (*PV-Cre*, 4 mice; *PV-Cre; Clock*$^{f/f}$, 3 mice) or adult ages (*PV-Cre*, 3 mice; *PV-Cre; Clock*$^{f/f}$, 6 mice). AU, arbitrary units. *$p < 0.05$; **$p < 0.01$ (two-way ANOVA, Bonferroni's post hoc analysis). Values are mean ± SEM.

(F and G) Immature Syt2 puncta onto pyramidal neurons in layer 4 of V1b in *PV-Cre; Clock*$^{f/f}$ mice at CP (P27). Cumulative plots for mean Syt2 puncta size per soma (F) and Syt2 puncta number per soma (G) and their mean values (insets) in *PV-Cre* (98 cells from 4 mice) and *PV-Cre; Clock*$^{f/f}$ mice (64 cells from 3 mice). ***$p < 0.001$ (K-S test for cumulative plots; Mann-Whitney test for insets).

(H) *Pvalb* expression in V1 of *Clock* or *Bmal1* conditional knockout mice at CP (P26–P28, 3–8 mice) or adult ages (P60–P90, 3–9 mice). **$p < 0.01$; ***$p < 0.001$ (two-way ANOVA, Bonferroni's post hoc analysis). Values are mean ± SEM.

(I) Reduced visual acuity after 4 days of monocular deprivation (MD) in *PV-Cre* controls during the CP (noMD and MD, 6 mice each) but not in adulthood (noMD and MD, 5 mice each). In contrast, a delayed CP plasticity is seen in adult *PV-Cre; Clock*$^{f/f}$ and *PV-Cre; Bmal1*$^{f/f}$ mice (noMD and MD, 5 mice each). **$p < 0.01$; ***$p < 0.001$; ns, not significant (t test). Values are mean ± SEM. See also Figures S6, S7, and S8.

Immunohistochemistry

Mice were anesthetized and then perfused transcardially with 4% (wt/vol) paraformaldehyde in 0.1 M phosphate buffer. Whole brains were removed, post-fixed for 3 hr, cryopreserved in 30% (wt/vol) sucrose in 0.1 M phosphate buffer, embedded in OCT compound (Sakura Finetek), and sectioned coronally on a Cryostat (Leica). Cryosections (35 μm) were blocked with buffer (10% normal goat serum and 0.1% Triton X-100 [vol/vol] in PBS) for 1 hr at room temperature. Incubation with primary antibodies in blocking buffer overnight at 4°C was followed by incubation with secondary antibodies. Stained sections were mounted and visualized using confocal microscopy (FV1000, Olympus).

Antibodies used in this study were rabbit anti-Parvalbumin (Swant, PV 25, 1:1,000), mouse anti-Parvalbumin (Swant, 235, 1:500), mouse anti-NeuN (Millipore, MAB377, 1:500), mouse anti-Synaptotagmin 2 (Developmental Studies Hybridoma Bank, znp-1, 1:250), rat anti-Somatostatin (Millipore, MAB354, 1:500), mouse anti-Calretinin (Swant, 6B3, 1:500), rabbit anti-PER1 (Millipore, AB2201, 1:5,000), rabbit anti-CLOCK (Millipore, AB2203, 1:5,000), guinea pig anti-BMAL1 (Millipore, AB2204, 1:5,000), mouse anti-CRE (Millipore, MAB3120, 1:200), and Alexa Fluor 488/594/647-conjugated goat anti-rabbit/mouse/rat/guinea pig IgG/IgG1/IgG2a (Molecular Probes, 1:400). Anti-PER1, anti-CLOCK, and anti-BMAL1 antibodies were made as described previously (Hastings et al., 1999; LeSauter et al., 2012). For staining of perineuronal nets, biotin-labeled lectin from *Wisteria Floribunda agglutinin* (WFA) (Sigma) and Alexa Fluor 488 Streptavidin (Molecular Probes, 1:400) were used.

Image Analysis

Image data were collected and analyzed blind to genotypes. Imaging settings were optimized and kept constant for the entire set of samples belonging to one experiment. To analyze PV cell and WFA-stained perineuronal nets, we

acquired images at 1,024 × 1,024 pixels using a 20× objective (0.75 numerical aperture) and analyzed in layers 2–5 of V1b with ImageJ. A threshold for PV cell somata was manually set for each image, such that all PV cell somata of different signal intensity were included and various background signals across images properly excluded. Then, somata were analyzed using the particle analysis function with >40 μm^2 as initial parameters. WFA mean intensity was measured after background subtraction. Percentage of WFA area was calculated from the WFA-positive area above a threshold (200 pixel intensity) from background intensity.

To analyze PV cell puncta, images were acquired at 1,024 × 1,024 pixels using a 100× oil-immersion objective (1.4 numerical aperture) and analyzed in layer 4 of V1b with ImageJ. Pyramidal cells were identified by NeuN immunoreactivity and their triangular shaped somata. Pyramidal cell soma were traced with a 2.25-μm-thick line (1 μm inside, 1.25 μm outside the soma edge), and PV puncta above a threshold (600 pixel intensity) within the trace were analyzed using the particle analysis function with 0.05–10 μm^2 as initial parameters. The threshold intensity was optimized for the entire set of images such that exclusion of low-intensity puncta (too high threshold) and fusion of multiple puncta (too low threshold) were minimized.

dLGN Segregation

Mice were anaesthetized with isoflurane. 1.5 μl of Cholera Toxin B subunit (CTB) conjugated to Alexa Fluor 488 was injected in the left eye and CTB conjugated to Alexa Fluor 594 was injected in the right eye (5 mg/ml dissolved in Saline; Molecular Probes). After 2 days, brains were processed in a same way as immunohistochemistry and sectioned coronally (100 μm) on a Cryostat (Leica). dLGN sections taken at the middle of the rostral-caudal extent of dLGN where the area of the ipsilateral eye projection is greatest were imaged using confocal microscopy (FV1000, Olympus). The degree of contralateral and ipsilateral eye axon overlap in dLGN was quantified using a multi-threshold protocol as previously described (Schafer et al., 2012; Torborg and Feller, 2004). The total area of overlapping pixels was represented as a percentage of total dLGN area.

PCR Genotyping

Genomic DNA was extracted from ear punches and PCR genotyping was performed using REDExtract-N-Amp Tissue PCR Kit (Sigma). Primers used in this study were described elsewhere (Debruyne et al., 2006; Storch et al., 2007).

Real-Time Quantitative RT-PCR

Total RNA was isolated from visual cortex with *mir*Vana miRNA Isolation Kit (Ambion), and any contaminating DNA was removed by TURBO DNA-*free* Kit (Invitrogen) according to manufacturer's instructions. First-strand cDNA was synthesized from total RNA using High Capacity RNA-to-cDNA Kit (Invitrogen) according to manufacturer's instructions. Real-time quantitative PCR was performed using TaqMan Gene Expression Assay (Applied Biosystems) on a StepOnePlus Real-Time PCR System (Applied Biosystems). TaqMan probes used in this study were for *Clock* (Mm00455950_m1), *Pvalb* (Mm00443100_m1), *Dbp* (Mm00497539_m1), *Per1* (Mm00501813_m1), *Per2* (Mm00478113_m1), *Clock* exon 5-6 (Mm00455940_g1), *Camk2a* (Mm00437967_m1), *Sst* (Mm00436671_m1), *Calb1* (Mm00486647_m1), *Calb2* (Mm00801461_m1), *Syt2* (Mm00436864_m1), and *Gapdh* (4352932E). Relative expression of target genes was determined by the $2^{-\Delta\Delta Ct}$ method (Livak and Schmittgen, 2001).

Monocular Deprivation Procedure

Eyelid margins were trimmed by iris scissor and eyelids sutured shut under isoflurane anesthesia, as described (Fagiolini et al., 2004; Fagiolini and Hensch, 2000; Sugiyama et al., 2008). Eyes were closed for 4 days from P25–P26 for critical period studies and from P60–P90 for adult studies. The integrity of the suture was checked daily and mice were used only if the eyelids remained closed throughout the duration of the deprivation period.

Visual Evoked Potential

Visual evoked potentials (VEPs) were recorded under nembutal/chlorprothixene anesthesia using standard techniques in mice (Fagiolini and Hensch, 2000; Porciatti et al., 1999). A tungsten electrode (9–12 MΩ) was inserted into V1b, where the maximal VEP response is located within the visual field 20° from the vertical meridian (3.0 mm from lambda) (Porciatti et al., 1999). Electrodes were advanced to a depth of 100–400 μm from the pial surface, where VEPs exhibit their maximal amplitude. Signals were band-pass filtered (0.1–100 Hz), amplified, and fed to a computer for analysis. In brief, at least 30 events were averaged in synchrony with abrupt stimulus contrast reversal (1 Hz). Transient VEPs were evaluated in the time domain by measuring the peak-to-baseline amplitude of the major negative component. Visual stimuli were horizontal sinusoidal gratings of different spatial frequencies at 100% contrast. Visual acuity was obtained by extrapolation to zero amplitude of the linear regression through the data points along a curve of VEP amplitude plotted against log spatial frequency. Ocular dominance was assessed by calculating the ratio of VEP amplitudes recorded by stimulating the eye contralateral and ipsilateral to the visual cortex where recording was performed.

Drug Administration

Diazepam (DZ, 2 mg/ml) or vehicle solution (Veh, 50% propylene glycol) were systemically injected (20 mg/kg, daily i.p.) under isoflurane anesthesia, starting 1 day before MD until the day before recording or over a 10-day period from P23 to P33 to restore an early "critical period" (Fagiolini and Hensch, 2000).

Acute Slice Electrophysiology

Animals anesthetized with isoflurane were quickly decapitated, their brains rapidly dissected, and 350-μm-thick coronal sections containing the V1 visual area collected using a blade microtome (Microm HM 650V, Thermo Scientific) in oxygenated (95% O_2, 5% CO_2) ice-cold cutting solution (Fagiolini and Hensch, 2000). Slices were incubated in artificial CSF (ACSF) at 34°C for 30 min and allowed to cool to room temperature. ACSF contained 125 mM NaCl, 2.5 mM KCl, 1.25 mM NaH_2PO_4, 2 mM $CaCl_2$, 1 mM $MgCl_2$, 25 mM glucose, and 25 mM $NaHCO_3$. Cutting solution contained 125 mM NaCl, 2.5 mM KCl, 1.25 mM NaH_2PO_4, 2 mM $CaCl_2$, 10 mM $MgCl_2$, 10 mM glucose, 25 mM $NaHCO_3$, and 4 mM Ascorbate. To assess intrinsic properties of PV cells, we performed whole-cell recordings with internal solution containing 130 mM K-gluconate, 4 mM KCl, 2 mM NaCl, 10 mM HEPES, 0.2 mM EGTA, 10 mM Phosphocreatine-Tris, 4 mM Mg-ATP, and 0.3 mM Na_3-GTP (Osmolarity 290 mOsm [pH = 7.2]).

For miniature inhibitory post-synaptic currents (mIPSCs), internal solution contained 100 mM KCl, 40 mM K-gluconate, 8 mM NaCl, 2 mM $MgCl_2$ 10 mM HEPES, 0.1 mM EGTA, 2 mM Mg-ATP, 0.3 mM Na_3-GTP, and 1 mM lidocaine derivative QX-314 (Osmolarity 290 mOsm [pH = 7.2]). Events were recorded at holding potential of −60 mV, with 20 μM CNQX (6-Cyano-7-nitro quinoxaline-2,3-dione disodium), 50 μM AP-5 (D-(-)-2-Amino-5- phosphonopentanoic acid), and 1 μM TTX (tetrodotoxin) added to the bath solution to block AMPA and NMDA receptors and voltage-gated sodium channels, respectively. At least 150-s-long traces were collected 3 min after break-in for mIPSC analysis. Whole-cell recordings were amplified using a Multiclamp 700B amplifier (Axon Instruments) and acquired using Clampex 10 and a Digidata 1440A board (Axon Instruments). Recordings were filtered at 10 kHz and digitized at 20 kHz. Liquid junction potentials were not compensated. Series resistance (5–12 MΩ) was closely monitored during recording. And recording was discarded if series resistance changed by >15%. Intrinsic properties were analyzed in Clampfit 10 (Axon Instruments). mIPSCs traces were after-filtered at 2 kHz and analyzed in mini-analysis (Synaptosoft). CNQX, AP-5, and TTX were purchased from Tocris Biosciences. All other chemicals were from Sigma-Aldrich.

Microarray Analysis

PV cells were isolated by following a trehalose-supplemented protocol (Saxena et al., 2012) from adult (P60–P64) *PV-GFP; Clock*$^{+/+}$ or *PV-GFP; Clock*$^{-/-}$ mice at ZT16. In brief, digestion and dissociation of dissected mouse cerebral cortex were performed using Papain Dissociation System (Worthington Biochemical Corporation) in the presence of 10% (vol/vol) D-trehalose (Sigma-Aldrich). Digested tissue was dissociated with measured trituration to obtain a single-cell suspension of mostly viable cells. The fluorescent PV cells in the resulting single-cell suspension were collected using MoFlo (Beckman Coulter) in the Bauer Core Facility at Harvard University and total RNA was extracted using TRIzol Reagent (Invitrogen) followed by RNeasy

Micro Kit (QIAGEN) with RNase-Free DNase Set (QIAGEN). RNA quality was assessed on a 2100 BioAnalyzer (Agilent Technologies).

For oligonucleotide microarray hybridization, 5 ng of total RNA were amplified with Ovation PicoSL WTA System V2 (NuGEN) and labeled with Encore BiotinIL Module (NuGEN). The resulting labeled cDNA was hybridized to MouseWG-6 v2.0 Expression BeadChip (Illumina). Preparation of cDNA and hybridization of cDNA to microarrays was conducted in the Boston Children's Hospital IDDRC Molecular Genetic Core Facility. The raw data were normalized by quantile normalization method with background subtraction using GenomeStudio Software (Illumina) and analyzed using GeneSpring GX 11 (Agilent Technologies). The differentially expressed genes ($p < 0.05$, $\log_2$-fold change >0.25 or <−0.25) were annotated with gene ontology (GO) terms (GOTERM_BP_FAT, GOTERM_CC_FAT, GOTERM_MF_FAT) and clustered using DAVID (Huang et al., 2009).

Statistical Analysis

All data are presented as mean ± SEM. Shapiro-Wilk test was used for normality. Two-tailed unpaired t test or Mann-Whitney test were used to compare between two groups. One-way ANOVA with Dunnett's multiple comparison test and two-way ANOVA with Bonferroni's multiple comparison test were used to compare multiple groups. Two-sample Kolmogorov-Smirnov test (K-S test) was used to compare the cumulative distributions of two groups. Statistical analyses were carried out with GraphPad Prism 5 (GraphPad Software) or SigmaPlot 12 (Systat Software).

ACCESSION NUMBERS

The NCBI GEO accession number for the microarray data reported in this paper is GSE62956.

SUPPLEMENTAL INFORMATION

Supplemental Information includes eight figures and one table and can be found with this article online at http://dx.doi.org/10.1016/j.neuron.2015.02.036.

AUTHOR CONTRIBUTIONS

Y.K. designed, performed, and analyzed most experiments. Z.Y. performed in vitro slice electrophysiology. T.K.H. supervised the project. Y.K. and T.K.H. wrote the paper.

ACKNOWLEDGMENTS

This work is dedicated to the memory of our dear colleague J. Woodland Hastings (1927–2014). We thank M. Nakamura for animal maintenance, E.Y. Litvina and E.K. Lehrman for assistance with dLGN segregation procedure and analysis, Y. Yoshihara for the *TLCN-Cre* line, all members of the T.K.H and M. Fagiolini laboratories for discussion, and NIMH Grant 1P50MH094271 (to T.K.H.) for support.

Received: June 15, 2014
Revised: January 25, 2015
Accepted: February 18, 2015
Published: March 19, 2015

REFERENCES

Allen, N.C., Bagade, S., McQueen, M.B., Ioannidis, J.P., Kavvoura, F.K., Khoury, M.J., Tanzi, R.E., and Bertram, L. (2008). Systematic meta-analyses and field synopsis of genetic association studies in schizophrenia: the SzGene database. Nat. Genet. *40*, 827–834.

Bartolini, G., Ciceri, G., and Marín, O. (2013). Integration of GABAergic interneurons into cortical cell assemblies: lessons from embryos and adults. Neuron *79*, 849–864.

Basu, S.N., Kollu, R., and Banerjee-Basu, S. (2009). AutDB: a gene reference resource for autism research. Nucleic Acids Res. *37*, D832–D836.

Beurdeley, M., Spatazza, J., Lee, H.H., Sugiyama, S., Bernard, C., Di Nardo, A.A., Hensch, T.K., and Prochiantz, A. (2012). Otx2 binding to perineuronal nets persistently regulates plasticity in the mature visual cortex. J. Neurosci. *32*, 9429–9437.

Bunger, M.K., Wilsbacher, L.D., Moran, S.M., Clendenin, C., Radcliffe, L.A., Hogenesch, J.B., Simon, M.C., Takahashi, J.S., and Bradfield, C.A. (2000). Mop3 is an essential component of the master circadian pacemaker in mammals. Cell *103*, 1009–1017.

Cabungcal, J.H., Steullet, P., Kraftsik, R., Cuenod, M., and Do, K.Q. (2013a). Early-life insults impair parvalbumin interneurons via oxidative stress: reversal by N-acetylcysteine. Biol. Psychiatry *73*, 574–582.

Cabungcal, J.H., Steullet, P., Morishita, H., Kraftsik, R., Cuenod, M., Hensch, T.K., and Do, K.Q. (2013b). Perineuronal nets protect fast-spiking interneurons against oxidative stress. Proc. Natl. Acad. Sci. USA *110*, 9130–9135.

Carulli, D., Pizzorusso, T., Kwok, J.C., Putignano, E., Poli, A., Forostyak, S., Andrews, M.R., Deepa, S.S., Glant, T.T., and Fawcett, J.W. (2010). Animals lacking link protein have attenuated perineuronal nets and persistent plasticity. Brain *133*, 2331–2347.

Chemerinski, E., Ho, B.C., Flaum, M., Arndt, S., Fleming, F., and Andreasen, N.C. (2002). Insomnia as a predictor for symptom worsening following antipsychotic withdrawal in schizophrenia. Compr. Psychiatry *43*, 393–396.

Chubykin, A.A., Atasoy, D., Etherton, M.R., Brose, N., Kavalali, E.T., Gibson, J.R., and Südhof, T.C. (2007). Activity-dependent validation of excitatory versus inhibitory synapses by neuroligin-1 versus neuroligin-2. Neuron *54*, 919–931.

Debruyne, J.P., Noton, E., Lambert, C.M., Maywood, E.S., Weaver, D.R., and Reppert, S.M. (2006). A clock shock: mouse CLOCK is not required for circadian oscillator function. Neuron *50*, 465–477.

Dibner, C., Schibler, U., and Albrecht, U. (2010). The mammalian circadian timing system: organization and coordination of central and peripheral clocks. Annu. Rev. Physiol. *72*, 517–549.

Dudley, C.A., Erbel-Sieler, C., Estill, S.J., Reick, M., Franken, P., Pitts, S., and McKnight, S.L. (2003). Altered patterns of sleep and behavioral adaptability in NPAS2-deficient mice. Science *301*, 379–383.

Fagiolini, M., and Hensch, T.K. (2000). Inhibitory threshold for critical-period activation in primary visual cortex. Nature *404*, 183–186.

Fagiolini, M., Fritschy, J.M., Löw, K., Möhler, H., Rudolph, U., and Hensch, T.K. (2004). Specific GABAA circuits for visual cortical plasticity. Science *303*, 1681–1683.

Gogolla, N., Leblanc, J.J., Quast, K.B., Südhof, T.C., Fagiolini, M., and Hensch, T.K. (2009). Common circuit defect of excitatory-inhibitory balance in mouse models of autism. J. Neurodev. Disord. *1*, 172–181.

Golombek, D.A., Bussi, I.L., and Agostino, P.V. (2014). Minutes, days and years: molecular interactions among different scales of biological timing. Philos. Trans. R. Soc. Lond. B Biol. Sci. *369*, 20120465.

Gonchar, Y., Wang, Q., and Burkhalter, A. (2007). Multiple distinct subtypes of GABAergic neurons in mouse visual cortex identified by triple immunostaining. Front. Neuroanat. *1*, 3.

Green, C.B., Durston, A.J., and Morgan, R. (2001). The circadian gene Clock is restricted to the anterior neural plate early in development and is regulated by the neural inducer noggin and the transcription factor Otx2. Mech. Dev. *101*, 105–110.

Grone, B.P., Chang, D., Bourgin, P., Cao, V., Fernald, R.D., Heller, H.C., and Ruby, N.F. (2011). Acute light exposure suppresses circadian rhythms in clock gene expression. J. Biol. Rhythms *26*, 78–81.

Hastings, M.H., Field, M.D., Maywood, E.S., Weaver, D.R., and Reppert, S.M. (1999). Differential regulation of mPER1 and mTIM proteins in the mouse suprachiasmatic nuclei: new insights into a core clock mechanism. J. Neurosci. *19*, RC11.

Hensch, T.K. (2004). Critical period regulation. Annu. Rev. Neurosci. *27*, 549–579.

Hensch, T.K. (2005). Critical period plasticity in local cortical circuits. Nat. Rev. Neurosci. *6*, 877–888.

Hensch, T.K., Fagiolini, M., Mataga, N., Stryker, M.P., Baekkeskov, S., and Kash, S.F. (1998). Local GABA circuit control of experience-dependent plasticity in developing visual cortex. Science *282*, 1504–1508.

Huang, Z.J., Kirkwood, A., Pizzorusso, T., Porciatti, V., Morales, B., Bear, M.F., Maffei, L., and Tonegawa, S. (1999). BDNF regulates the maturation of inhibition and the critical period of plasticity in mouse visual cortex. Cell *98*, 739–755.

Huang, W., Sherman, B.T., and Lempicki, R.A. (2009). Systematic and integrative analysis of large gene lists using DAVID bioinformatics resources. Nat. Protoc. *4*, 44–57.

Huberman, A.D., Feller, M.B., and Chapman, B. (2008). Mechanisms underlying development of visual maps and receptive fields. Annu. Rev. Neurosci. *31*, 479–509.

Janich, P., Pascual, G., Merlos-Suárez, A., Batlle, E., Ripperger, J., Albrecht, U., Cheng, H.Y., Obrietan, K., Di Croce, L., and Benitah, S.A. (2011). The circadian molecular clock creates epidermal stem cell heterogeneity. Nature *480*, 209–214.

Kang, E., Durand, S., LeBlanc, J.J., Hensch, T.K., Chen, C., and Fagiolini, M. (2013). Visual acuity development and plasticity in the absence of sensory experience. J. Neurosci. *33*, 17789–17796.

Kobayashi, Y., and Hensch, T.K. (2013). Germline recombination by conditional gene targeting with Parvalbumin-Cre lines. Front. Neural Circuits *7*, 168.

Kondratov, R.V., Kondratova, A.A., Gorbacheva, V.Y., Vykhovanets, O.V., and Antoch, M.P. (2006). Early aging and age-related pathologies in mice deficient in BMAL1, the core componentof the circadian clock. Genes Dev. *20*, 1868–1873.

Le Magueresse, C., and Monyer, H. (2013). GABAergic interneurons shape the functional maturation of the cortex. Neuron *77*, 388–405.

LeSauter, J., Lambert, C.M., Robotham, M.R., Model, Z., Silver, R., and Weaver, D.R. (2012). Antibodies for assessing circadian clock proteins in the rodent suprachiasmatic nucleus. PLoS ONE *7*, e35938.

Livak, K.J., and Schmittgen, T.D. (2001). Analysis of relative gene expression data using real-time quantitative PCR and the 2(-Delta Delta C(T)) Method. Methods *25*, 402–408.

Lowrey, P.L., and Takahashi, J.S. (2011). Genetics of circadian rhythms in Mammalian model organisms. Adv. Genet. *74*, 175–230.

Madisen, L., Zwingman, T.A., Sunkin, S.M., Oh, S.W., Zariwala, H.A., Gu, H., Ng, L.L., Palmiter, R.D., Hawrylycz, M.J., Jones, A.R., et al. (2010). A robust and high-throughput Cre reporting and characterization system for the whole mouse brain. Nat. Neurosci. *13*, 133–140.

Marcheva, B., Ramsey, K.M., Buhr, E.D., Kobayashi, Y., Su, H., Ko, C.H., Ivanova, G., Omura, C., Mo, S., Vitaterna, M.H., et al. (2010). Disruption of the clock components CLOCK and BMAL1 leads to hypoinsulinaemia and diabetes. Nature *466*, 627–631.

Marín, O. (2012). Interneuron dysfunction in psychiatric disorders. Nat. Rev. Neurosci. *13*, 107–120.

Masri, S., and Sassone-Corsi, P. (2010). Plasticity and specificity of the circadian epigenome. Nat. Neurosci. *13*, 1324–1329.

Maya Vetencourt, J.F., Sale, A., Viegi, A., Baroncelli, L., De Pasquale, R., O'Leary, O.F., Castrén, E., and Maffei, L. (2008). The antidepressant fluoxetine restores plasticity in the adult visual cortex. Science *320*, 385–388.

Meyer, A.H., Katona, I., Blatow, M., Rozov, A., and Monyer, H. (2002). In vivo labeling of parvalbumin-positive interneurons and analysis of electrical coupling in identified neurons. J. Neurosci. *22*, 7055–7064.

Mitsui, S., Saito, M., Mori, K., and Yoshihara, Y. (2007). A transcriptional enhancer that directs telencephalon-specific transgene expression in mouse brain. Cereb. Cortex *17*, 522–530.

Mongrain, V., La Spada, F., Curie, T., and Franken, P. (2011). Sleep loss reduces the DNA-binding of BMAL1, CLOCK, and NPAS2 to specific clock genes in the mouse cerebral cortex. PLoS ONE *6*, e26622.

Morgan, R. (2002). The circadian gene Clock is required for the correct early expression of the head specific gene Otx2. Int. J. Dev. Biol. *46*, 999–1004.

Morishita, H., and Hensch, T.K. (2008). Critical period revisited: impact on vision. Curr. Opin. Neurobiol. *18*, 101–107.

Morishita, H., Miwa, J.M., Heintz, N., and Hensch, T.K. (2010). Lynx1, a cholinergic brake, limits plasticity in adult visual cortex. Science *330*, 1238–1240.

Morishita, H., Cabungcal, J.-H., Chen, Y., Do, K.Q., and Hensch, T.K. (2015). Prolonged period of cortical plasticity upon redox dysregulation in fast-spiking interneurons. Biol Psych. Published online January 24, 2015. http://dx.doi.org/10.1016/j.biopsych.2014.12.026.

Musiek, E.S., Lim, M.M., Yang, G., Bauer, A.Q., Qi, L., Lee, Y., Roh, J.H., Ortiz-Gonzalez, X., Dearborn, J.T., Culver, J.P., et al. (2013). Circadian clock proteins regulate neuronal redox homeostasis and neurodegeneration. J. Clin. Invest. *123*, 5389–5400.

Paschos, G.K., Ibrahim, S., Song, W.L., Kunieda, T., Grant, G., Reyes, T.M., Bradfield, C.A., Vaughan, C.H., Eiden, M., Masoodi, M., et al. (2012). Obesity in mice with adipocyte-specific deletion of clock component Arntl. Nat. Med. *18*, 1768–1777.

Pizzorusso, T., Medini, P., Berardi, N., Chierzi, S., Fawcett, J.W., and Maffei, L. (2002). Reactivation of ocular dominance plasticity in the adult visual cortex. Science *298*, 1248–1251.

Plessy, C., Fagiolini, M., Wagatsuma, A., Harasawa, N., Kuji, T., Asaka-Oba, A., Kanzaki, Y., Fujishima, S., Waki, K., Nakahara, H., et al. (2008). A resource for transcriptomic analysis in the mouse brain. PLoS ONE *3*, e3012.

Porciatti, V., Pizzorusso, T., and Maffei, L. (1999). The visual physiology of the wild type mouse determined with pattern VEPs. Vision Res. *39*, 3071–3081.

Saxena, A., Wagatsuma, A., Noro, Y., Kuji, T., Asaka-Oba, A., Watahiki, A., Gurnot, C., Fagiolini, M., Hensch, T.K., and Carninci, P. (2012). Trehalose-enhanced isolation of neuronal sub-types from adult mouse brain. Biotechniques *52*, 381–385.

Schafer, D.P., Lehrman, E.K., Kautzman, A.G., Koyama, R., Mardinly, A.R., Yamasaki, R., Ransohoff, R.M., Greenberg, M.E., Barres, B.A., and Stevens, B. (2012). Microglia sculpt postnatal neural circuits in an activity and complement-dependent manner. Neuron *74*, 691–705.

Shapiro-Reznik, M., Jilg, A., Lerner, H., Earnest, D.J., and Zisapel, N. (2012). Diurnal rhythms in neurexins transcripts and inhibitory/excitatory synapse scaffold proteins in the biological clock. PLoS ONE *7*, e37894.

Shearman, L.P., Sriram, S., Weaver, D.R., Maywood, E.S., Chaves, I., Zheng, B., Kume, K., Lee, C.C., van der Horst, G.T., Hastings, M.H., and Reppert, S.M. (2000). Interacting molecular loops in the mammalian circadian clock. Science *288*, 1013–1019.

Shimomura, H., Moriya, T., Sudo, M., Wakamatsu, H., Akiyama, M., Miyake, Y., and Shibata, S. (2001). Differential daily expression of Per1 and Per2 mRNA in the suprachiasmatic nucleus of fetal and early postnatal mice. Eur. J. Neurosci. *13*, 687–693.

Sommeijer, J.P., and Levelt, C.N. (2012). Synaptotagmin-2 is a reliable marker for parvalbumin positive inhibitory boutons in the mouse visual cortex. PLoS ONE *7*, e35323.

Southwell, D.G., Froemke, R.C., Alvarez-Buylla, A., Stryker, M.P., and Gandhi, S.P. (2010). Cortical plasticity induced by inhibitory neuron transplantation. Science *327*, 1145–1148.

Spatazza, J., Lee, H.H., Di Nardo, A.A., Tibaldi, L., Joliot, A., Hensch, T.K., and Prochiantz, A. (2013). Choroid-plexus-derived Otx2 homeoprotein constrains adult cortical plasticity. Cell Rep. *3*, 1815–1823.

Storch, K.F., Paz, C., Signorovitch, J., Raviola, E., Pawlyk, B., Li, T., and Weitz, C.J. (2007). Intrinsic circadian clock of the mammalian retina: importance for retinal processing of visual information. Cell *130*, 730–741.

Südhof, T.C. (2008). Neuroligins and neurexins link synaptic function to cognitive disease. Nature *455*, 903–911.

Sugiyama, S., Di Nardo, A.A., Aizawa, S., Matsuo, I., Volovitch, M., Prochiantz, A., and Hensch, T.K. (2008). Experience-dependent transfer of

Otx2 homeoprotein into the visual cortex activates postnatal plasticity. Cell *134*, 508–520.

Takahashi, J.S., Hong, H.K., Ko, C.H., and McDearmon, E.L. (2008). The genetics of mammalian circadian order and disorder: implications for physiology and disease. Nat. Rev. Genet. *9*, 764–775.

Torborg, C.L., and Feller, M.B. (2004). Unbiased analysis of bulk axonal segregation patterns. J. Neurosci. Methods *135*, 17–26.

Wakamatsu, H., Yoshinobu, Y., Aida, R., Moriya, T., Akiyama, M., and Shibata, S. (2001). Restricted-feeding-induced anticipatory activity rhythm is associated with a phase-shift of the expression of mPer1 and mPer2 mRNA in the cerebral cortex and hippocampus but not in the suprachiasmatic nucleus of mice. Eur. J. Neurosci. *13*, 1190–1196.

Weber, E.T., and Andrade, R. (2010). Htr2a gene and 5-HT(2A) receptor expression in the cerebral cortex studied using genetically modified mice. Front Neurosci *4*, 36.

Wiesel, T.N. (1982). Postnatal development of the visual cortex and the influence of environment. Nature *299*, 583–591.

Wulff, K., Gatti, S., Wettstein, J.G., and Foster, R.G. (2010). Sleep and circadian rhythm disruption in psychiatric and neurodegenerative disease. Nat. Rev. Neurosci. *11*, 589–599.

Yagita, K., Horie, K., Koinuma, S., Nakamura, W., Yamanaka, I., Urasaki, A., Shigeyoshi, Y., Kawakami, K., Shimada, S., Takeda, J., and Uchiyama, Y. (2010). Development of the circadian oscillator during differentiation of mouse embryonic stem cells in vitro. Proc. Natl. Acad. Sci. USA *107*, 3846–3851.

Yan, L., Miyake, S., and Okamura, H. (2000). Distribution and circadian expression of dbp in SCN and extra-SCN areas in the mouse brain. J. Neurosci. Res. *59*, 291–295.

Yu, X., Rollins, D., Ruhn, K.A., Stubblefield, J.J., Green, C.B., Kashiwada, M., Rothman, P.B., Takahashi, J.S., and Hooper, L.V. (2013). TH17 cell differentiation is regulated by the circadian clock. Science *342*, 727–730.